International Journal of Pharmaceutics: X 6 (2023) 100218

Contents lists available at ScienceDirect

International Journal of Pharmaceutics: X

journal homepage: www.sciencedirect.com/journal/international-journal-of-pharmaceutics-x

Polydopamine-activated celastrol carbon dots for synergistic chemotherapy-photothermal therapy of tumors

Ping Sheng, Chao Bu, Tanyue Hui, Lili Zhou, Hao Chen *, Guoliang Zhou *

College of life and Health Sciences, Anhui Science and Technology University, Fengyang, 233100, China

ARTICLE INFO

Keywords:
Polydopamine
Celastrol carbon dots
Carbon dots combined polydopamine
Chemotherapy-photothermal synergistic therapy

ABSTRACT

Synergistic chemotherapy and photothermal therapy (PTT) holds the promise of addressing the weakness of individualized chemotherapy and PTT. In this study, we synthesized a chemotherapeutic agent, PDA-Ce-CDs, which combines the photothermal conversion ability and the generation of hydroxyl radicals (•OH), enabling synergistic enhancement of antitumor effects. Furthermore, the localized heating effect of NIR radiation promoted the uptake of the PDA-Ce-CDs and enhances the sensitivity of intracellular reactive oxygen species (ROS). Finally, the antitumor activity of the PDA-Ce-CDs was evaluated through cell experiments and tumor-bearing mice experiments, confirming its excellent antitumor efficacy *in vivo* and *in vitro*. Our work presents a new strategy in cancer treatment by utilizing carbon dots in combination with photothermal agents for synergistic chemotherapy-photothermal therapy. This innovative approach offers a new therapeutic avenue for synergistic tumor treatment by harnessing the combined effects of photothermal therapy and chemotherapy.

1. Introduction

Cancer is universally recognized as a severe and lethal disease, with a sustained increase in its incidence in recent years, posing a grave threat to human health (Chen and Zhang, 2020; Guo et al., 2022; Hosseini et al., 2023). Chemotherapy is one of the most widely used therapeutic methods in clinical practice, effectively suppressing tumor proliferation and extending the life of patients (Chabner and Roberts, 2005; Song et al., 2022). However, most conventional chemotherapy drugs are often limited by a lack of tumor site specificity and selectivity, which could result in suboptimal treatment outcomes (Feng et al., 2020a). From a developmental perspective, achieving significant anti-tumor effects with a single therapy is challenging. Thus, cancer treatment is gradually transitioning from monotherapy to combination therapy (Ding et al., 2017; Li and Lin, 2023; *Nat. Biomed. Eng.*, 2018; Shim et al., 2017). The emergence of nanocarrier platforms has provided new possibilities for the in-depth exploration of tumor therapeutic strategies (Butowska et al., 2023; Feng et al., 2022).

PTT, relying on near-infrared (NIR) laser irradiation to generate therapeutic heat (Duan et al., 2023; Zhi et al., 2020). The temperature elevation enhances the generation and diffusion of reactive oxygen species (ROS), leading to cell membrane disruption and thus achieving synergistic therapy (Liu et al., 2020). Polydopamine (PDA) (Xu et al., 2023) exhibits excellent biocompatibility and remarkable photothermal conversion efficiency, making it an excellent photothermal agent (Huang et al., 2019). Moreover, the surface of PDA existed numerous functional groups, allowing for covalent conjugation with other materials through addition reactions (Lu et al., 2021a; Ma et al., 2019; Wu et al., 2022). However, the therapeutic efficacy of PTT is limited by the penetration depth of light. Fortunately, combination therapy allows for the synergistic integration of multiple therapeutic modalities, which goes beyond the simple summation of individual treatment effects and instead harnesses a synergistic effect, thus enhancing therapeutic efficacy (Duan et al., 2023; Yang et al., 2023).

Celastrol (Ce), as a potential chemotherapeutic agent, has been discovered to disrupt the proliferation and invasion processes of multiple cancer cells, thereby inhibiting tumor growth and metastasis (Hsieh et al., 2019; Medatwal et al., 2020; Xiao et al., 2018). However, its clinical application is limited due to drawbacks such as low bioavailability and poor water solubility (Ge et al., 2020). Considering the unique characteristics of carbon dots (Lu et al., 2021b) (easy modification, excellent photoluminescent properties, high water solubility, low cytotoxicity, and good biocompatibility), we propose the preparation of Ce carbon dots (Ce-CDs) to mitigate the limitations associated with the standalone use of Ce for antitumor applications (Chai et al., 2022; Ding et al., 2017; Li et al., 2019; Zhou et al., 2016).

* Corresponding authors.
E-mail addresses: chenhao@ahstu.edu.cn (H. Chen), zhouguoliang96@126.com (G. Zhou).

https://doi.org/10.1016/j.ijpx.2023.100218
Received 14 August 2023; Received in revised form 8 October 2023; Accepted 7 November 2023
Available online 8 November 2023

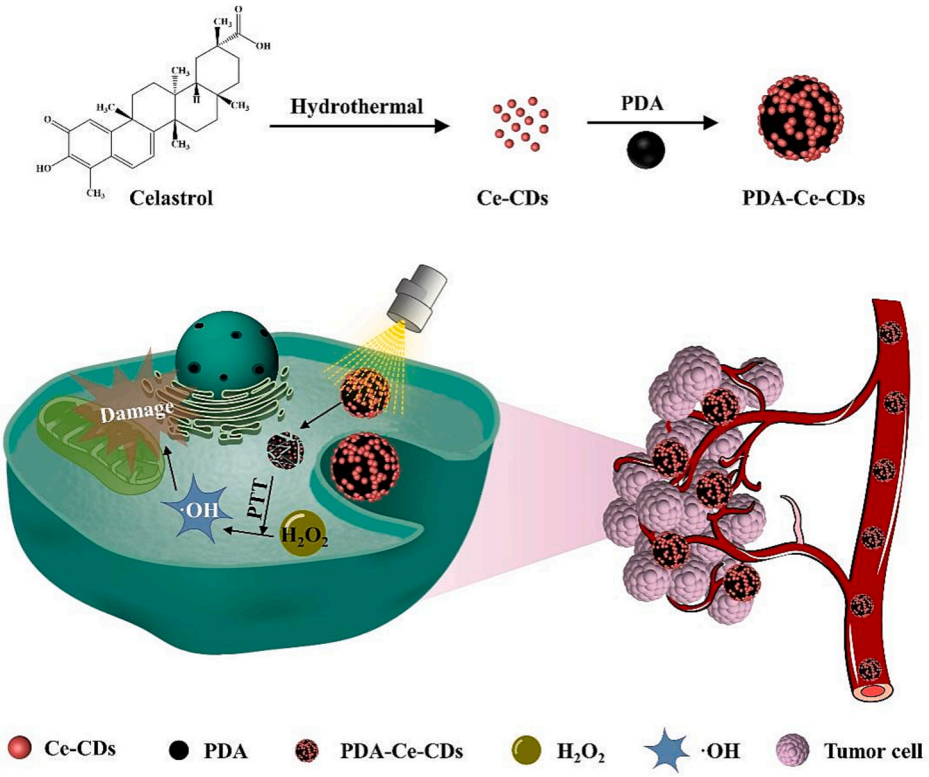

Scheme 1. Steps of synthesizing PDA-Ce-CDs and antitumor mechanism.

Inspired by synergistic therapy, in this study, we constructed a platform for synergistic chemotherapy-photothermal therapy (Scheme 1). The Ce-CDs were synthesized through a hydrothermal reaction, while retaining the anticancer activity of Ce. Subsequently, the Ce-CDs were conjugated to the surface of the photothermal agent (PDA), through an amide reaction. The resulting the PDA-Ce-CDs exhibited excellent photothermal performance attributed to their strong NIR absorption capacity, enabling efficient light-to-heat conversion for PTT. Under NIR irradiation, the PDA-Ce-CDs demonstrated excellent peroxidase-like activity, effectively catalyzing endogenous H_2O_2 generation to produce •OH for inducing cancer cells. Moreover, the amide bonds were cleaved, facilitating drug release. *In vitro* and *in vivo* experiments demonstrated the superior therapeutic efficacy of the PDA-Ce-CDs, enabling synergistic photothermal therapy, controlled drug release, and ROS generation.

2. Experimental part

2.1. Materials

Celastrol (Ce) and dopamine hydrochloride (DA) were purchased from Aladdin Biochemical Technology Co., Ltd. (Shanghai, China). Cell culture reagents were obtained from Thermo Fisher Scientific Co., Ltd. (Shanghai, China). ROS assay kits, fluorescent dyes, and Annexin V-FITC/PI apoptosis detection kits were all bought from wanlei Biotechnology Co., Ltd. (Shenyang, China).

2.2. Preparation of PDA-Ce-CDs

The preparation of PDA-Ce-CDs involves three steps. In the first step, Ce-CDs were synthesized using a one-pot hydrothermal method. Briefly, 0.4 g of Ce was dispersed in 10 mL of water and heated at 200 °C for 24 h. Subsequently, the suspension was placed in a dialysis membrane (MWCO = 500 Da) and dialyzed for 24 h with deionized water changed every 3 h (He et al., 2018). Finally, Ce-CDs were obtained by freeze-drying. In the second step, common synthetic methods were employed to prepare PDA nanoparticles (Liu et al., 2013; Lu et al., 2019). In the third step, Ce-CDs were loaded onto the surface of PDA nanoparticles. Briefly, the Ce-CDs were added to the aqueous solution of PDA, stirred overnight, and the final product was collected and named PDA-Ce-CDs.

2.3. Characterization of PDA-Ce-CDs

The morphology of PDA-Ce-CDs was obtained using TEM (Hitachi, Japan). FTIR was used to record the structural properties and functional groups of Ce, Ce-CDs, and PDA-Ce-CDs using an IRTracer-100 instrument (Japan). The elemental composition of PDA-Ce-CDs was determined by XPS (Escalab 250Xi, Thermo Fisher Scientific Nexsa, USA).

2.4. The photothermal performance of PDA-Ce-CDs

To investigate the photothermal properties of PDA-Ce-CDs, we irradiated them with infrared light of varying power densities. Additionally, we exposed solutions containing different concentrations of PDA-Ce-CDs or different materials (Ce, Ce-CDs, and PDA-Ce-CDs) to 808 nm laser radiation for 5 min in centrifuge tubes. We also studied the photothermal stability of PDA-Ce-CDs by subjecting them to repeated irradiation with 808 nm near-infrared laser until a specific temperature was reached. The temperature of PDA-Ce-CDs at different points was measured using an infrared thermal imager (TiS55, Fluke, USA).

2.5. Hemolytic assays

Specimens for hemolysis experiments were obtained from ICR mice (Li et al., 2020). The erythrocytes with or without PDA-Ce-CDs solution (0, 50, 100, 200, 400, and 800 μg/mL) were prepared and incubated at 37 °C for 3 h. The absorbance of the supernatant was measured at 540 nm and the percentage of hemolysis was calculated with the following formula: $Hemolysis(\%) = \frac{OD_{540\ GEPP-CDs} - OD_{540\ PBS}}{OD_{540\ deionized\ water} - OD_{540\ PBS}} \times 100\%$.

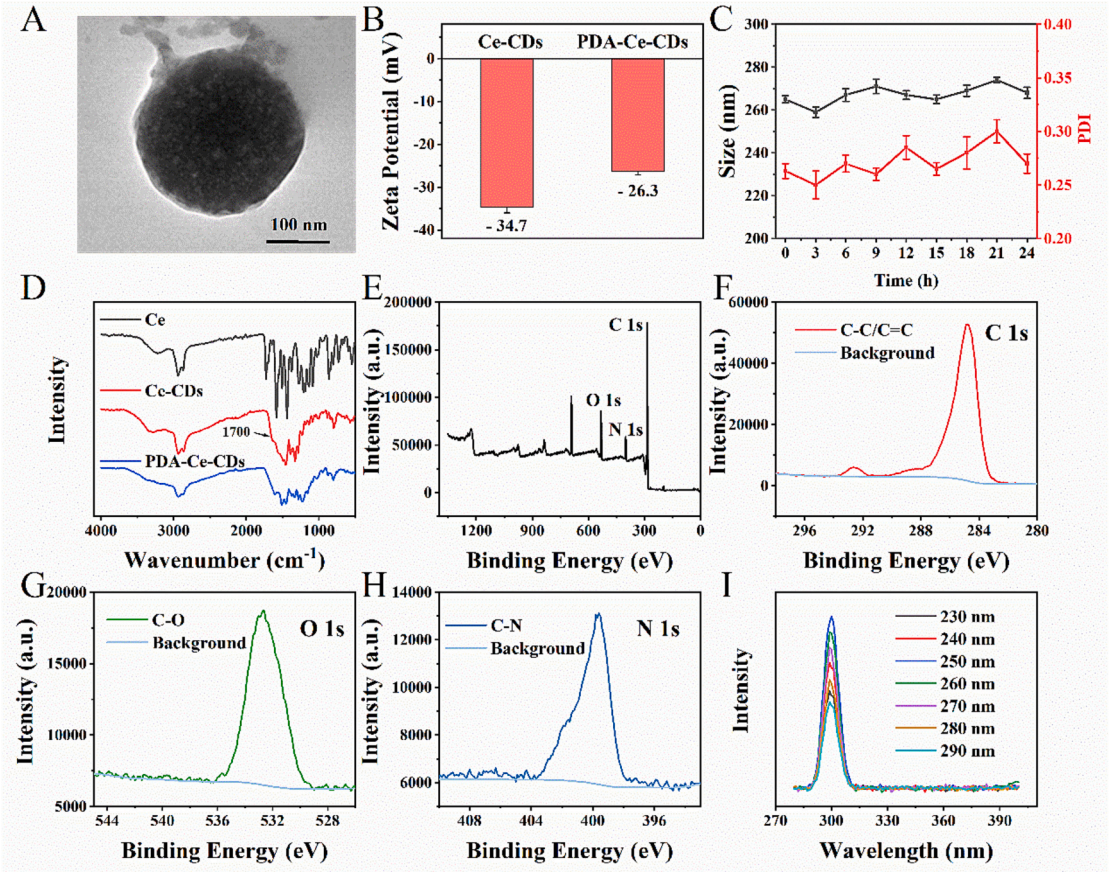

Fig. 1. (A) TEM images of the PDA-Ce-CDs. (B) Zeta potentials results. (C) Size and PDI results in pH 7.4 PBS. (D) FTIR spectrum. (E) XPS survey scan spectrum. (F) C 1 s, (G) O 1 s, and (H) N 1 s high-resolution XPS spectra. (I) Fluorescence emission spectra of the PDA-Ce-CDs.

2.6. Cytotoxicity study in vitro

The cytotoxicity of PDA-Ce-CDs on 4 T1 cells was assessed using the MTT assay. The cells were treated with different concentrations (0, 0.625, 1.25, 2.5, 5, 10 μg/mL) of Ce, Ce-CDs, and PDA-Ce-CDs for 24 h under both light and dark conditions. After the treatment, the absorbance at 492 nm was measured using an ELISA reader. Under light conditions, 4 T1 cells were subjected to 808 nm laser irradiation for 5 min.

2.7. Cellular uptake

Cellular uptake behavior of PDA-Ce-CDs was investigated by utilizing CLSM (Hou et al., 2021). ICG-PDA-Ce-CDs were prepared by mixing PDA-Ce-CDs with ICG solution and stirring for 2 h. The 4 T1 cells (1×10^5 cells per well) were seeded in culture dishes and incubated with ICG-PDA -Ce-CDs. The irradiation group was subjected to 5 min of cell irradiation. The cellular uptake of ICG-PDA-Ce-CDs was observed at 0, 2, and 6 h.

2.8. Intracellular hydroxyl radicals (•OH) detection

The PDA-Ce-CDs were co-incubated with 4 T1 cells for 12 h. The NIR irradiation group were exposed to 808 nm laser irradiation after 4 h, followed by a 30 min incubation in culture medium containing DCFH-DA. Finally, fluorescent images of the intracellular contents were obtained.

2.9. Cell apoptosis test

After incubation with or without PDA-Ce-CDs for 2 h, the 4 T1 cells were exposed to the NIR irradiation for 3 min, and stained with Annexin V-FITC/PI for readily FCM analysis.

2.10. Antitumor effect study in vivo

Animal experiments were conducted following the guidelines set by the Animal Ethics Committee of Anhui Science and Technology University. BALB/c mice were injected with 100 μL of 4 T1 cell suspension (approximately 5×10^6 cells) in the axillary region to establish the 4 T1 tumor-bearing mouse model. When the tumor size reached about 0.1 cm^3, the tumor-bearing mice were randomly divided into four groups ($n = 8$): (1) saline, (2) Ce-CDs, (3) PDA-Ce-CDs, (4) PDA-Ce-CDs + laser (laser irradiation conditions: 808 nm, 1.5 W/cm^2, 5 min). The tumor-bearing mice were intravenously injected with a dose of 10 mg/kg (100 μL) every 3 days, and the mice in the laser irradiation group underwent laser irradiation 12 h after injection. Tumor volume and body weight were recorded, and the volume (V) was calculated using the formula V = (tumor length) × (tumor width)^2/2.

3. Results and discussion

3.1. Preparation and characterization of PDA-Ce-CDs

The preparation process of PDA-Ce-CDs is shown in Scheme 1. Ce-CDs were synthesized by a hydrothermal method, and they were loaded onto the surface of PDA through an amide reaction. The high-resolution electron microscopy showed that Ce-CDs had a smooth and

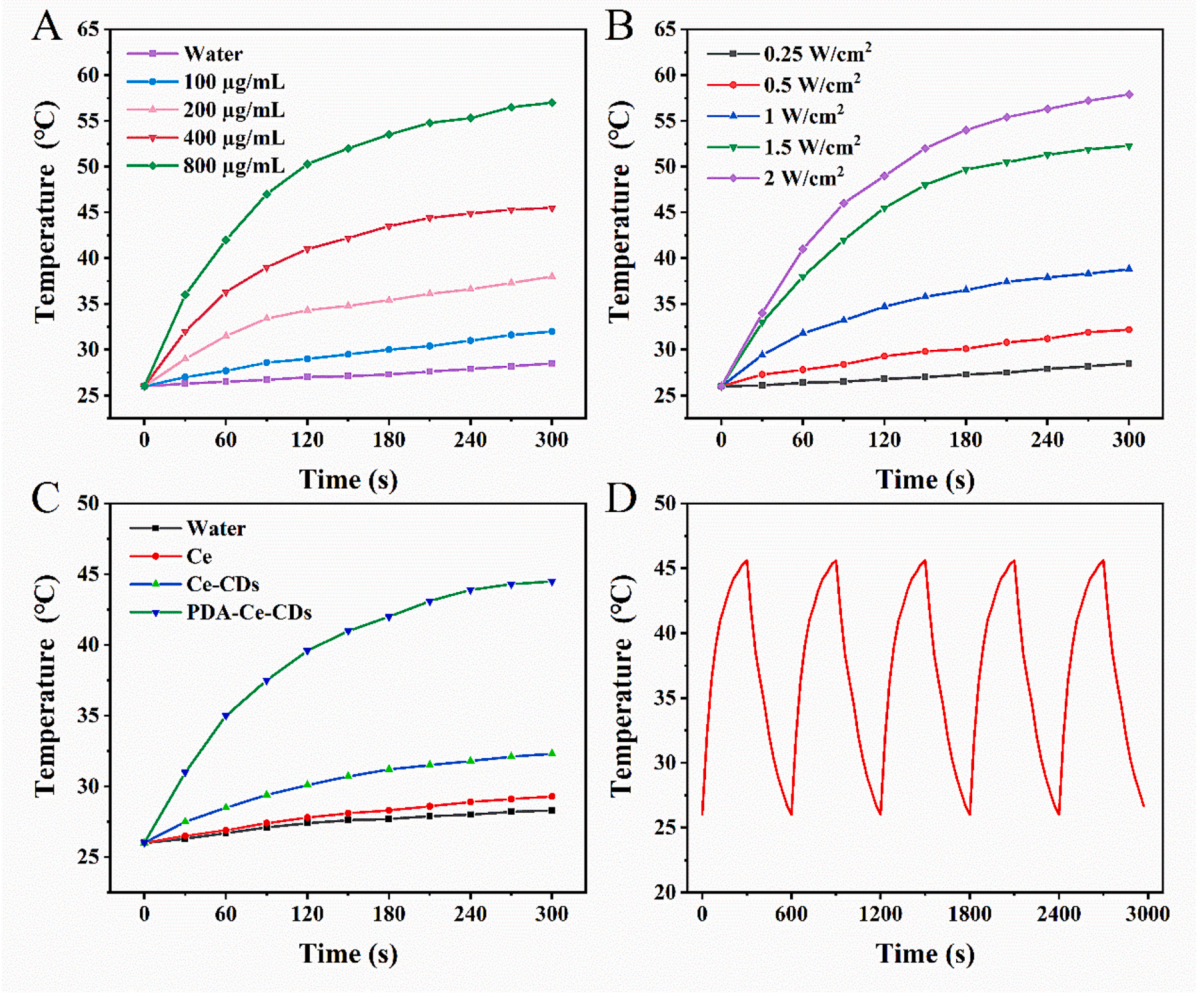

Fig. 2. Temperature variation curves of (A) gradient concentrations of the PDA-Ce-CDs; (B) Different laser powers of the PDA-Ce-CDs. (C) Temperature elevation profile of the aqueous dispersion of the water, the Ce, the Ce-CDs, and the PDA-Ce-CDs under NIR irradiation. (D) Photothermal stability of the PDA-Ce-CDs.

uniform surface with an average diameter of 9.2 nm (Fig. S2 and Fig. S3), and PDA-Ce-CDs had a dispersed quasi-spherical shape with an average particle size of 260 nm (Fig. 1A and C). Moreover, the Zeta potentials of Ce-CDs and PDA-Ce-CDs were measured to be −34.7 mV and − 26.3 mV (Fig. 1B), respectively. The increase in potential after PDA encapsulation was attributed to the presence of amino functional groups in the chemical structure of PDA. The chemical properties of GEPP-CDs were characterized using FTIR (Lu et al., 2021a), and the encapsulation of PDA was achieved through an amide reaction, which involved the coupling of the amino groups of PDA with the carboxyl groups on the surface of Ce-CDs. The disappearance of the stretching vibration peak of -COOH at 1700 cm^{-1} (Fig. 1D) confirmed the transformation of carboxyl groups into amide bonds. Additionally, XPS spectra were recorded to analyze the chemical composition and bonding states of PDA-Ce-CDs (Fig. 1E). The particles were composed of carbon, oxygen, and nitrogen, with binding energies at 286, 531, and 400 eV, corresponding to atomic contents of 73.89%, 11.29%, and 14.83%, respectively. The high-resolution C 1 s (Fig. 1F), O 1 s (Fig. 1G), and N 1 s (Fig. 1H) peaks appeared at 284.8, 532.6, and 399.6 eV, corresponding to C-C/C=C, C═O, and C—N bonds, respectively, indicating the presence of amide bonds in PDA-Ce-CDs (Chu et al., 2020; Hao et al., 2021; Zhao et al., 2019). The XPS analysis results were consistent with the FTIR results, confirming the successful synthesis of PDA-Ce-CDs. The optical properties of PDA-Ce-CDs were investigated using the fluorescence (FL) spectrum (Fig. 1I), revealing strong fluorescence intensity at 303 nm when excited at a wavelength of 250 nm.

3.2. *In vitro photothermal effect*

To investigate the photothermal effect of PDA-Ce-CDs nanoparticles, we irradiated them with infrared light at different power densities and concentrations. The temperature changes were monitored, and the results showed a concentration-dependent, irradiation time-dependent, and power density-dependent pattern of photothermal effects (Fig. 2A and B). To study the photothermal properties induced by near-infrared laser irradiation, we measured the temperature increase of Ce, Ce-CDs, and PDA-Ce-CDs under irradiation to examine the photothermal properties of different materials. Ce-CDs showed a slight temperature increase during irradiation, while PDA-Ce-CDs showed a significant increase, and no obvious heating was observed in Ce or water (Fig. 2C). In addition, we evaluated the photothermal stability of PDA-Ce-CDs by subjecting them to five on/off cycles of continuous 808 nm laser irradiation for 5 min per cycle (Fig. 2D). The temperature curves and peak shapes showed no significant changes before and after the cyclic laser exposure, indicating that PDA-Ce-CDs exhibit good photostability.

3.3. *In vitro hemolysis assay*

The red blood cells in DI water would rapidly swell and fracture, while in sterile saline solutions without or with different concentrations of the PDA-Ce-CDs erythrocytes maintained their integrity (Fig. 3C). The hemolysis percentage rate was only 4.3% (< 5%) at 800 μg/mL of the GEPP-CDs (Fig. 3D). Furthermore, reducing the concentration of PDA-

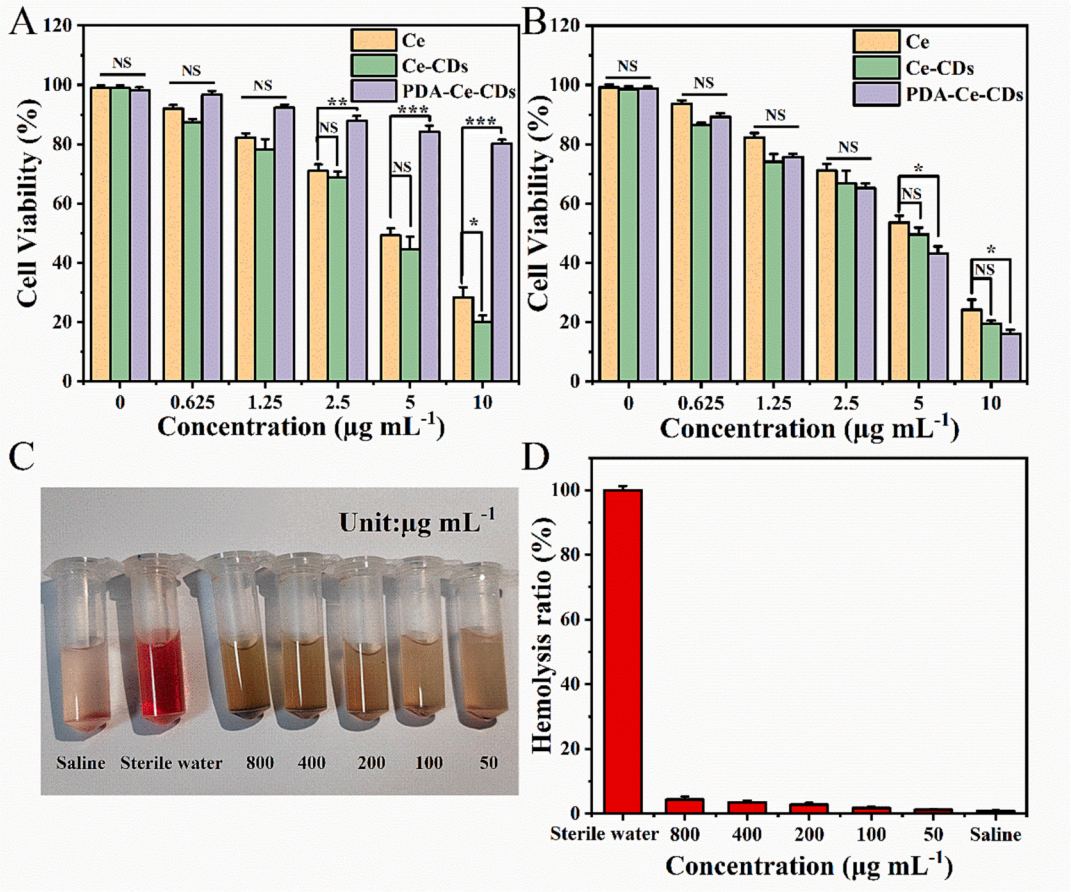

Fig. 3. Cell viability of 4 T1 cells without (A) and with (B) NIR laser irradiation. Images of hemolysis (C) and hemolysis ratio (D) of different concentrations of the PDA-Ce-CDs on red blood cells. *$p < 0.05$, **$p < 0.01$ and ***$p < 0.001$. (For interpretation of the references to colour in this figure legend, the reader is referred to the web version of this article.)

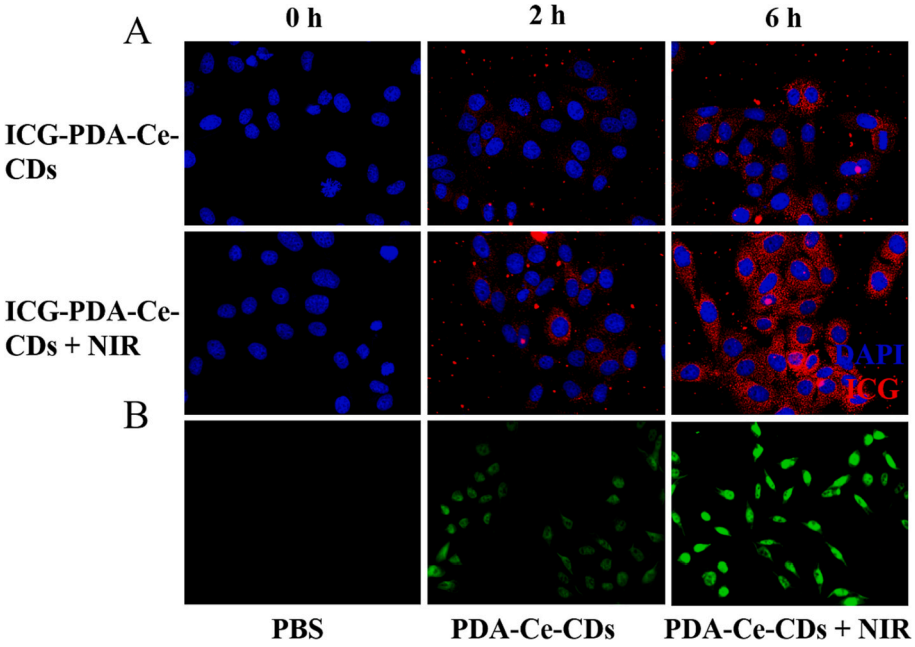

Fig. 4. (A) *In vitro* cellular uptake with and without NIR irradiation after being treated by the ICG-PDA-Ce-CDs for 0, 2, and 6 h. (B) Intracellular ROS labeled by the DCFH fluorescence probe.

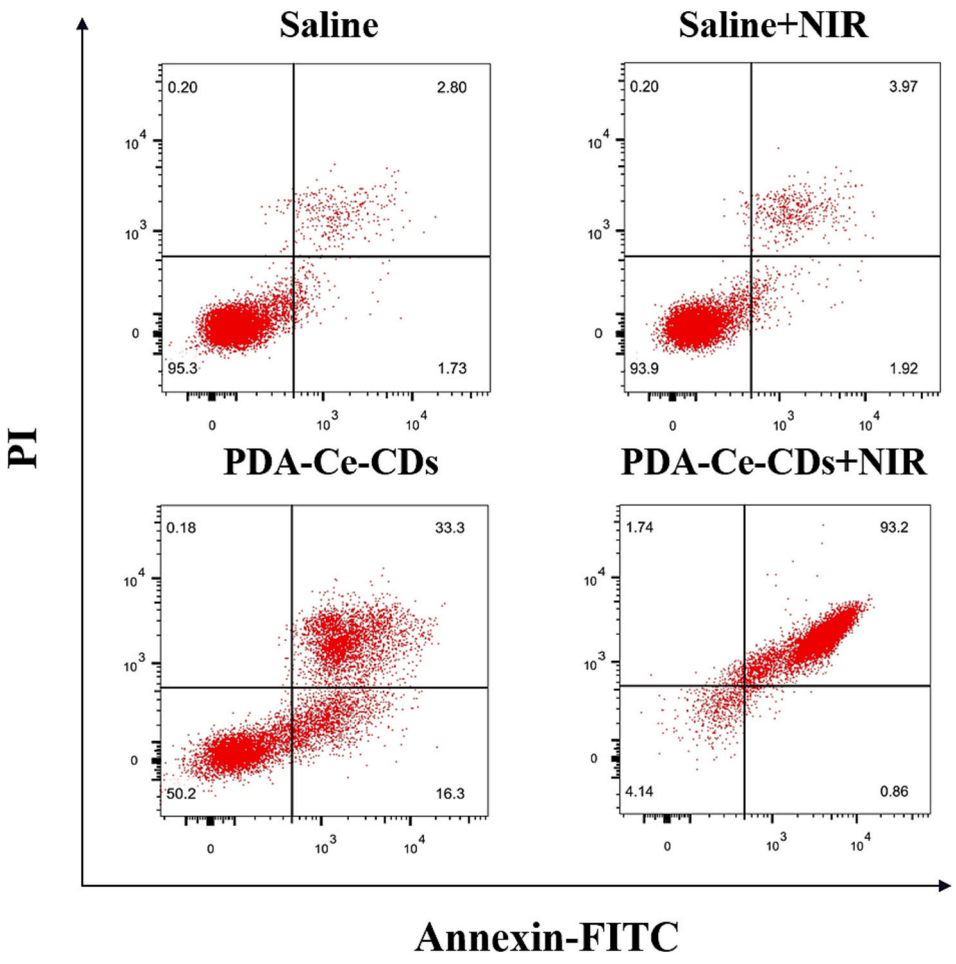

Fig. 5. Different groups of induced 4 T1 cells were analyzed for apoptosis using Annexin V-FITC/PI staining.

Ce-CDs results in a lower rate of hemolysis. These results indicated the excellent blood biocompatibility of the PDA-Ce-CDs.

3.4. Cytotoxicity test

In the absence of laser irradiation (Fig. 3A), Ce and Ce-CDs showed strong inhibitory effects on 4 T1 cells in the experimental concentration range, with cell survival rates of 28.4% and 20.1%, respectively, when the concentration was 10 μg/mL, which demonstrated the superior antitumor effects of Ce-CDs relative to Ce. While the introduction of PDA into the preparation of PDA-Ce-CDs showed higher cell survival (>80%), indicating its good safety and biocompatibility. Under laser irradiation conditions (Fig. 3B), the cell viability significantly decreased with increasing concentrations of PDA-Ce-CDs, indicating its excellent photothermal conversion feature. Expectedly, at a dosage of 10 μg/mL, PDA-Ce-CDs exhibited higher cytotoxicity under near-infrared light irradiation compared to Ce and Ce-CDs, indicating the effective tumor cell-killing potential of chemotherapy and photothermal synergistic therapy.

3.5. Cellular uptake assay

According to reports, photothermal could enhance the cellular uptake of drugs (Feng et al., 2020b). To confirm the cellular uptake of PDA-Ce-CDs, we loaded indocyanine green (ICG) as an indicator and loaded it onto PDA-Ce-CDs, resulting in the synthesis of ICG-PDA-Ce-CDs. The 4 T1 cells were treated by the ICG-PDA-Ce-CDs (with or without NIR laser irradiation) and examined at 0, 2, and 6 h after incubation. As shown in Fig. 4A, the intracellular endocytosis of ICG-PDA-Ce-CDs started to occur under laser irradiation after 2 h, and this effect became more pronounced with the prolongation of time (after 6 h). It should be noted that the ICG-PDA-Ce-CDs + NIR group exhibited the highest red fluorescence, indicating that ICG-PDA-Ce-CDs were more prone to cellular internalization under near-infrared illumination. As shown in Fig. 4B, the 4 T1 cells treated with PDA-Ce-CDs exhibited intense green fluorescence, indicating the generation of a substantial amount of •OH within the cells by PDA-Ce-CDs, thereby inducing oxidative stress. As expected, laser irradiation significantly enhanced the green fluorescence of cells treated with PDA-Ce-CDs, which could be attributed to the decomposition of PDA-Ce-CDs and the exposure of Ce-CDs under laser irradiation, thereby leading to increased production of •OH.

3.6. Cell apoptosis test

FCM was employed to measure the apoptosis rate, exploring the synergistic mechanisms of the PDA-Ce-CDs in chemo-photothermal therapy. As shown in Fig. 5, the PDA-Ce-CDs group exhibited about 16% of cells in the early apoptotic stage and about 33% in the late apoptotic stage. This phenomenon could be attributed to the intrinsic chemotherapeutic effect of the PDA-Ce-CDs and its ability to generate a large amount of free radicals, thereby disrupting mitochondrial function and inducing cell apoptosis. However, the cells in PBS and PBS + NIR groups exhibited no observable apoptosis phenomenon, indicating the safety of NIR laser irradiation for normal biological tissues. Significantly, the apoptosis rate in the PDA-Ce-CDs + NIR group increased to 93%, providing strong evidence for the potent synergistic antitumor effect of PDA-Ce-CDs with chemical photothermal therapy.

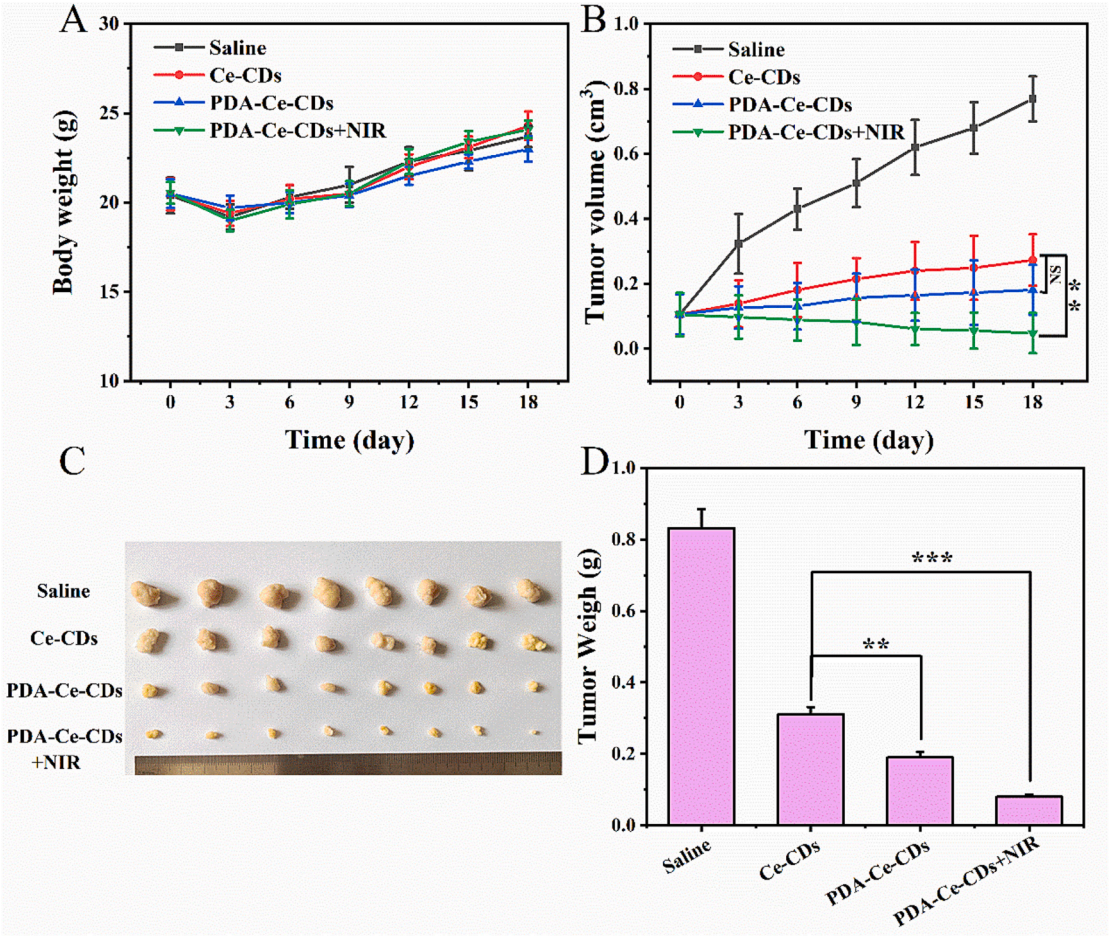

Fig. 6. (A) Body weight of different groups in the therapeutic period. (B) Change in tumor volume 18 days after various treatments. (C) Photos of *ex vivo* tumors in different treatment groups. (D) Mean weight of tumor. $^{**}p < 0.01$ and $^{***}p < 0.001$.

3.7. In vivo antitumor therapy

To further investigate the anti-tumor effect of PDA-Ce-CDs, we established a 4 T1 tumor model (Yun et al., 2022). As shown in Fig. 6B, the saline group exhibited rapid tumor growth, while both the Ce-Cd-Cd group and PDA-Ce-Cd group demonstrated a certain degree of tumor inhibition. In contrast, the PDA-Ce-CDs + NIR group demonstrated a pronounced inhibitory effect. Furthermore, as evidenced by the typical photographs of tumors (Fig. 6C) and tumor weight measurements (Fig. 6D) taken after 18 days of treatment, the antitumor effect of PDA-Ce-CDs was enhanced under NIR irradiation, further confirming the remarkable efficacy of PDA-Ce-CDs in synergistic photothermal-chemotherapy. The intrinsic chemotherapeutic effect and the ROS-responsive drug release properties of PDA-Ce-CDs are the primary reasons for its antitumor efficacy. Moreover, PDA-Ce-CDs demonstrate efficient photothermal effects under laser irradiation, leading to an elevation of intracellular reactive oxygen species in tumor cells, which also contributes to its antitumor activity. Concurrently, the body weight of the mice was monitored throughout the treatment period, and it remained stable (Fig. 6A), indicating that PDA-Ce-CDs had low systemic toxicity and good biocompatibility.

4. Conclusions

In summary, we have successfully synthesized PDA-activated PDA-Ce-CDs based on the synergistic chemotherapy-photothermal therapy strategy, which not only possess superior optical properties but also retain the antitumor activity of Ce. Under NIR laser irradiation, the PDA-Ce-CDs could induce temperature elevation, promote drug release and cellular uptake, enabling the integration of photothermal therapy and chemotherapy to effectively eliminate tumors. *In vivo* tumor-bearing mice experiments and *in vitro* cell experiments demonstrate the excellent antitumor efficacy of PDA-Ce-CDs. Taken together, this platform that synergistically enhances the antitumor effects through the combination of carbon dots and photothermal agents presents a promising prospect for our fight against cancer.

Credit author statement

(First Author): Ping Sheng: Experimental design, Writing, Experiments, Methodology.
Chao Bu: Data curation, Experiments.
Tanyue Hui: Investigation, Visualization.
Lili Zhou: Data curation.
(Corresponding Author):
Guoliang Zhou: Experimental design, Resources, Supervision.
Hao Chen: Experimental design, Resources, Supervision.

Declaration of Competing Interest

The authors declare that they have no competing interests.

Data availability

The authors do not have permission to share data.

Acknowledgments

This work was financially supported by the Anhui Science and Technology University School-level Natural Project (2021zryb22) and the Anhui Provincial Department of Education Natural Research Project (KJ2021A0882).

Appendix A. Supplementary data

Supplementary data to this article can be found online at https://doi.org/10.1016/j.ijpx.2023.100218.

References

Butowska, K., Han, X., Gong, N., El-Mayta, R., Haley, R.M., Xue, L., Zhong, W., Guo, W., Wang, K., Mitchell, M.J., 2023. Doxorubicin-conjugated siRNA lipid nanoparticles for combination cancer therapy. Acta Pharm. Sin. B 13 (4), 1429–1437.

Chabner, B.A., Roberts, T.G., 2005. Chemotherapy and the war on cancer. Nat. Rev. Cancer 5 (1), 65–72.

Chai, Y., Feng, Y., Zhang, K., Li, J., 2022. Preparation of fluorescent carbon dots composites and their potential applications in biomedicine and drug delivery—a review. Pharmaceutics 14 (11), 2482.

Chen, X., Zhang, Y., 2020. Combination of tumor fragments and nanotechnology as a therapeutic approach: Treating a tumor with tumor. Nano Today 35, 100993.

Chu, X., Wu, F., Sun, B., Zhang, M., Song, S., Zhang, P., Wang, Y., Zhang, Q., Zhou, N., Shen, J., 2020. Genipin cross-linked carbon dots for antimicrobial, bioimaging and bacterial discrimination. Colloids Surf. B: Biointerfaces 190, 110930.

Ding, H., Wei, J.-S., Zhong, N., Gao, Q.-Y., Xiong, H.-M., 2017. Highly efficient red-emitting carbon dots with gram-scale yield for bioimaging. Langmuir 33 (44), 12635–12642.

Duan, S., Hu, Y., Zhao, Y., Tang, K., Zhang, Z., Liu, Z., Wang, Y., Guo, H., Miao, Y., Du, H., Yang, D., Li, S., Zhang, J., 2023. Nanomaterials for photothermal cancer therapy. RSC Adv. 13 (21), 14443–14460.

Feng, S., Mao, Y., Wang, X., Zhou, M., Lu, H., Zhao, Q., Wang, S., 2020a. Triple stimuli-responsive ZnO quantum dots-conjugated hollow mesoporous carbon nanoplatform for NIR-induced dual model antitumor therapy. J. Colloid Interface Sci. 559, 51–64.

Feng, S., Mao, Y., Wang, X., Zhou, M., Lu, H., Zhao, Q., Wang, S., 2020b. Triple stimuli-responsive ZnO quantum dots-conjugated hollow mesoporous carbon nanoplatform for NIR-induced dual model antitumor therapy. J. Colloid Interface Sci. 559, 51–64.

Feng, S., Lu, J., Wang, K., Di, D., Shi, Z., Zhao, Q., Wang, S., 2022. Advances in smart mesoporous carbon nanoplatforms for photothermal–enhanced synergistic cancer therapy. Chem. Eng. J. 435, 134886.

Ge, P., Niu, B., Wu, Y., Xu, W., Li, M., Sun, H., Zhou, H., Zhang, X., Xie, J., 2020. Enhanced cancer therapy of celastrol in vitro and in vivo by smart dendrimers delivery with specificity and biosafety. Chem. Eng. J. 383, 123228.

Guo, F., Yang, Z., Sehouli, J., Kaufmann, A.M., 2022. Blockade of ALDH in Cisplatin-Resistant Ovarian Cancer Stem Cells In Vitro Synergistically Enhances Chemotherapy-Induced Cell Death, 29(4), pp. 2808–2822.

Hao, X., Huang, L., Zhao, C., Chen, S., Lin, W., Lin, Y., Zhang, L., Sun, A., Miao, C., Lin, X., Chen, M., Weng, S., 2021. Antibacterial activity of positively charged carbon quantum dots without detectable resistance for wound healing with mixed bacteria infection. Mater. Sci. Eng. C Mater. Biol. Appl. 123, 111971.

He, M., Zhang, J., Wang, H., Kong, Y., Xiao, Y., Xu, W., 2018. Material and optical properties of fluorescent carbon quantum dots fabricated from lemon juice via hydrothermal reaction. Nanoscale Res. Lett. 13 (1), 175.

Hosseini, S.M., Mohammadnejad, J., Salamat, S., Beiram Zadeh, Z., Tanhaei, M., Ramakrishna, S., 2023. Theranostic polymeric nanoparticles as a new approach in cancer therapy and diagnosis: a review, Materials Today. Chemistry 29, 101400.

Hou, M., Zhong, Y., Zhang, L., Xu, Z., Kang, Y., Xue, P., 2021. Polydopamine (PDA)-activated cobalt sulfide nanospheres responsive to tumor microenvironment (TME) for chemotherapeutic-enhanced photothermal therapy. Chin. Chem. Lett. 32 (3), 1055–1060.

Hsieh, M.-J., Wang, C.-W., Lin, J.-T., Chuang, Y.-C., Hsi, Y.-T., Lo, Y.-S., Lin, C.-C., Chen, M.-K., 2019. Celastrol, a plant-derived triterpene, induces cisplatin-resistance nasopharyngeal carcinoma cancer cell apoptosis though ERK1/2 and p38 MAPK signaling pathway. Phytomedicine 58, 152805.

Huang, X., Wu, J., He, M., Hou, X., Wang, Y., Cai, X., Xin, H., Gao, F., Chen, Y., 2019. Combined cancer chemo-photodynamic and photothermal therapy based on ICG/PDA/TPZ-loaded nanoparticles. Mol. Pharm. 16 (5), 2172–2183.

Li, Y., Lin, W., 2023. Platinum-based combination nanomedicines for cancer therapy. Curr. Opin. Chem. Biol. 74, 102290.

Li, W., Liu, Y., Wang, B., Song, H., Liu, Z., Lu, S., Yang, B., 2019. Kilogram-scale synthesis of carbon quantum dots for hydrogen evolution, sensing and bioimaging. Chin. Chem. Lett. 30 (12), 2323–2327.

Li, L., Liu, H., Bian, J., Zhang, X., Fu, Y., Li, Z., Wei, S., Xu, Z., Liu, X., Liu, Z., Wang, D., Gao, D., 2020. Ag/Pd bimetal nanozyme with enhanced catalytic and photothermal effects for ROS/hyperthermia/chemotherapy triple-modality antitumor therapy. Chem. Eng. J. 397.

Liu, Y., Ai, K., Liu, J., Deng, M., He, Y., Lu, L., 2013. Dopamine-melanin colloidal nanospheres: an efficient near-infrared photothermal therapeutic agent for in vivo cancer therapy. Adv. Mater. 25 (9), 1353–1359.

Liu, Y., Shi, Q., Zhang, Y., Jing, J., Pei, J., 2020. One-step facile synthesis of Au@copper–tannic acid coordination core–shell nanostructures as photothermally-enhanced ROS generators for synergistic tumour therapy. New J. Chem. 44 (44), 19262–19269.

Lu, Q., Qi, S., Li, P., Yang, L., Yang, S., Wang, Y., Cheng, Y., Song, Y., Wang, S., Tan, F., Li, N., 2019. Photothermally activatable PDA immune nanomedicine combined with PD-L1 checkpoint blockade for antimetastatic cancer photoimmunotherapy. J. Mater. Chem. B 7 (15), 2499–2511.

Lu, J., Wang, K., Lei, W., Mao, Y., Di, D., Zhao, Q., Wang, S., 2021a. Polydopamine-carbon dots functionalized hollow carbon nanoplatform for fluorescence-imaging and photothermal-enhanced thermochemotherapy. Mater. Sci. Eng. C Mater. Biol. Appl. 122, 111908.

Lu, J., Wang, K., Lei, W., Mao, Y., Di, D., Zhao, Q., Wang, S., 2021b. Polydopamine-carbon dots functionalized hollow carbon nanoplatform for fluorescence-imaging and photothermal-enhanced thermochemotherapy. Mater. Sci. Eng. C 122, 111908.

Ma, H., Li, S., Zhang, H., Wei, Y., Jiang, L., 2019. Fabrication of polydopamine-based layer-by-layer nanocomposites for combined pH-sensitive chemotherapy and photothermal therapy. Colloids Surf. A Physicochem. Eng. Asp. 561, 332–340.

Medatwal, N., Ansari, M.N., Kumar, S., Pal, S., Jha, S.K., Verma, P., Rana, K., Dasgupta, U., Bajaj, A., 2020. Hydrogel-mediated delivery of celastrol and doxorubicin induces a synergistic effect on tumor regression via upregulation of ceramides. Nanoscale 12 (35), 18463–18475.

Powerful combination therapies. Nat. Biomed. Eng. 2 (8), 2018, 555–556.

Shim, G., Kim, M.-G., Kim, D., Park, J.Y., Oh, Y.-K., 2017. Nanoformulation-based sequential combination cancer therapy. Adv. Drug Deliv. Rev. 115, 57–81.

Song, G., Liang, G., Tian, T., Zhang, X., 2022. Mathematical Modeling and Analysis of Tumor Chemotherapy, Symmetry.

Wu, Y., Zhang, X., Tan, B., Shan, Y., Zhao, X., Liao, J., 2022. Near-infrared light control of GelMA/PMMA/PDA hydrogel with mild photothermal therapy for skull regeneration. Biomater. Adv 133, 112641.

Xiao, Y., Liu, J., Guo, M., Zhou, H., Jin, J., Liu, J., Liu, Y., Zhang, Z., Chen, C., 2018. Synergistic combination chemotherapy using carrier-free celastrol and doxorubicin nanocrystals for overcoming drug resistance. Nanoscale 10 (26), 12639–12649.

Xu, H., Zhang, Y., Zhang, H., Zhang, Y., Xu, Q., Lu, J., Feng, S., Luo, X., Wang, S., Zhao, Q., 2023. Smart polydopamine-based nanoplatforms for biomedical applications: state-of-art and further perspectives. Coord. Chem. Rev. 488, 215153.

Yang, W., Hu, H., Pan, Q., Deng, X., Zhang, Y., Shao, Z., 2023. Iron-polydopamine coated multifunctional nanoparticle SiO2@PDA/Fe3+-FA mediated low temperature photothermal for chemodynamic therapy of cisplatin-insensitive osteosarcoma. Mater. Des. 227.

Yun, K., Guo, J., Zhu, R., Wang, T., Zhang, X., Pan, H., Pan, W., 2022. Design of ROS-Responsive Hyaluronic Acid-Methotrexate Conjugates for Synergistic Chemo-Photothermal Therapy for Cancer. Mol. Pharm. 19 (9), 3323–3335.

Zhao, C., Wang, X., Wu, L., Wu, W., Zheng, Y., Lin, L., Weng, S., Lin, X., 2019. Nitrogen-doped carbon quantum dots as an antimicrobial agent against Staphylococcus for the treatment of infected wounds. Colloids Surf. B: Biointerfaces 179, 17–27.

Zhi, D., Yang, T., O'Hagan, J., Zhang, S., Donnelly, R.F., 2020. Photothermal therapy. J. Control. Release 325, 52–71.

Zhou, J., Deng, W., Wang, Y., Cao, X., Chen, J., Wang, Q., Xu, W., Du, P., Yu, Q., Chen, J., Spector, M., Yu, J., Xu, X., 2016. Cationic carbon quantum dots derived from alginate for gene delivery: One-step synthesis and cellular uptake. Acta Biomater. 42, 209–219.